Available online at www.sciencedirect.com

jmr&t Journal of Materials Research and Technology

journal homepage: www.elsevier.com/locate/jmrt

Original Article

# Determination of tensile behavior of hot-pressed Mg–$TiO_2$ and Mg–$ZrO_2$ nanocomposites using indentation test and a holistic inverse modeling technique

*Kaveh Rahmani* [a,*], *Alireza Nouri* [b,c], *Greg Wheatley* [d], *Hossein Malekmohammadi* [a], *Hamed Bakhtiari* [a], *Vahid Yazdi* [e]

[a] *Department of Mechanical Engineering, Bu-Ali Sina University, Hamedan, Iran*
[b] *School of Engineering, RMIT University, Melbourne, VIC, Australia*
[c] *Biomedical Engineering Department, Amirkabir University of Technology (Tehran Polytechnic), Tehran, Iran*
[d] *College of Science & Engineering, James Cook University, James Cook Dr, Douglas, QLD 4811, Australia*
[e] *Department of Mechanical Engineering, Kar Higher Education Institute of Qazvin, Qazvin, Iran*

ARTICLE INFO

*Article history:*
Received 25 May 2021
Accepted 19 July 2021
Available online 29 July 2021

*Keywords:*
Mg–$ZrO_2$ nanocomposites
Mg–$TiO_2$ nanocomposites
Tensile properties
Indentation
Finite element
Neural networks

ABSTRACT

The present study aims to implement a non-destructive approach to determine the tensile properties of magnesium-based nanocomposites reinforced with $ZrO_2$ and $TiO_2$ nanoparticles. Micron-sized magnesium particles were blended with 0, 1.5, 3, and 5 volume percentage of $ZrO_2$ and $TiO_2$ nanoparticles and hot-pressed at 450 °C under the pressure of 600 MPa. Next, the spherical indentation test was performed on the produced composites to obtain the load–penetration curves. A finite element model of the indentation test was then developed using the Hollomon material model with randomly chosen materials constants. At the next stage, load–penetration curves were obtained for each composite using simulations. A Levenberg–Marquardt neural network was then trained and utilized to find the correct material constants by minimizing the differences between the experimental and simulated load–penetration curves. The results indicated that there is a linear relationship between the tensile strength and content of the reinforcement phase, while it is inversely proportional to the size of the reinforcing particles. Magnesium composites reinforced with 5 volume percentage of $ZrO_2$ and $TiO_2$ nanoparticles showed tensile strengths 2.5 and 2.1 times greater than that of unreinforced magnesium, respectively. It was shown that the proposed method is able to calculate the tensile properties of magnesium-based composites in an accurate and inexpensive manner.



* Corresponding author.
E-mail addresses: k.rahmani@basu.ac.ir, rahmanii.kaveh@gmail.com (K. Rahmani).
https://doi.org/10.1016/j.jmrt.2021.07.090

## 1. Introduction

Metal matrix composites (MMCs) have found widespread application in automotive [1,2], aerospace [3], biomedical [4,5], and microelectronic industries [6]. MMCs have superior strength-to-weight ratio compared to their constituent elements. Downsizing the reinforcement phase to nano-scale further improves their mechanical properties [7,8]. Powder metallurgy (PM) is the most common fabrication method for producing metal matrix nanocomposites (MMNCs) [9]. Different PM techniques such as quasi-static compaction and dynamic compaction methods can be used for this purpose [10–12]. Hot pressing and cold pressing–sintering [13–15] and hot extrusion [16] are among the most commonly used quasi-static techniques. Due to the brittle and porous nature of metal matrix composites reinforced with ceramic materials, their tensile and compressive strengths are not equal. To date, most of the previous studies have investigated the compressive strength of such composites [17]. The reason is that the composite samples produced by the PM routes are usually small for tensile testing; thus, some non-destructive [18,19] and semi-destructive [20,21] techniques are needed for this purpose. It has been shown that the tensile strength and hardness of a material are interdependent on each other. Researchers have examined various experimental approaches to develop a mathematical relationship between the hardness and the yield strength of materials [22]. In 1951, Tabor firstly investigated the relationship between the Vickers (HV) or Brinell (HB) hardness and the yield stress ($\sigma_y$) as HV $\approx 3\,\sigma_y$ and HB $\approx 2.8\,\sigma_y$, respectively [23,24]. Lai and Lim [25] examined the relationship between the hardness and tensile properties of some steel grades. They found that the strain hardening coefficient and strength of all tested materials are linearly related to the hardness, regardless of the measurement method. The load (L)–penetration depth (P) curves obtained from the indentation experiments have also been extensively used for estimating the tensile stress–strain curves of various materials [20,25,26]. It has been proven that the penetration depth strongly depends on the elastoplastic behavior of materials. Converting the L–P curve into the stress–strain curve has been studied by researchers [27]. Noii and Aghayan [28] performed indentation tests on thin film coating materials and obtained the elastic–plastic deformation by minimizing the least squares error between the experimental data and the finite element (FE) results. Aiming at reducing the computational time in FE analysis and numerical optimization loop, Chen et al. [29] introduced a database of simulated indentation force–depth curves to extract the tensile strength and successfully examined their approach on eight materials.

Artificial neural networks (ANNs) have been successfully and widely implemented in surrogate modeling of various mechanical characterization problems [30–33]. In comparison with analytical approaches, ANN modeling requires no prior mathematical formulation of the problem. Besides, correlations between the indentation L–P curves and tensile properties are highly nonlinear due to the geometric, materials, and surface contact nonlinearities. Thus, analytical and semi-empirical methods fail to recognize all nonlinear parameters, leading to invalid or less accurate results. ANNs, if well architectured and adjusted, can automatically develop an accurate mathematical model of highly-nonlinear problems. In previous studies [21,34–36] an alternative approach that uses spherical indentation tests, FE simulation, and neural networks, has been successfully implemented to determine the Hollomon equation's coefficients. Kucharski and Mróz [37] carried out a similar investigation to measure the yield stress and strain-hardening parameters. However, a study conducted by Atrian et al. [35] on Al7075-SiC nanocomposites is the only published work in the literature that implemented the FE-ANN-Indentation method for mechanical characterization of composites. This is of particular importance for composite materials produced by the powder compaction techniques, as the size of the samples produced by these methods at laboratory scales does not allow for standard tensile testing. Therefore, more investigations are required to examine the efficacy of the proposed approach for metallic composites fabricated by the PM techniques.

In the present research, a combined FE-ANN-Indentation technique was utilized for tensile characterization of magnesium (Mg) based composites for the first time. One can determine the tensile properties by simulating the indentation test with FE software and extract the unknown constants of the implemented material model, thorough minimizing the differences between the experimental and simulated L–P curves. The Hollomon material model is a well-known equation that incorporates the material's hardening effects. A typical L–P curve consists of two paths: loading and unloading. Some researchers have used the slope of the loading and the unloading parts in the L–P curve to evaluate the plastic behavior and Young's modulus of materials, respectively [21,23,24,26]. Although this approach is a fairly complicated and time-consuming process, it is still a reliable, efficient, and inexpensive method, and is the only available method to evaluate the tensile properties of miniature specimens. However, such empirical equations usually are valid only for certain groups of materials. To address this challenge, in this paper, a non-destructive semi-empirical approach based on the spherical indentation test is introduced for evaluating the tensile strength of Mg–$TiO_2$ and Mg–$ZrO_2$ nanocomposites produced by the PM technique. Spherical indentation tests were carried out on the produced samples to obtain the experimental L–P curves. A FE-neural network framework was then utilized to find the tensile strengths of the composites.

## 2. Experiments and methods

Magnesium powder (purity 99%, 63 μm) was mixed with 0, 1.5, 3, and 5 volume percentage (vol.%) of titanium oxide (purity 99%, 10–25 nm) and zirconium oxide (purity 99.95%, 20 nm) nanoparticles. The fabrication stages and parameters in this article were adopted according to the investigations conducted by the authors in their previous study [38]. To obtain a uniform dispersion of particles, the powder mixture was milled in a planetary ball mill (NARYA-MPM 4 × 250). To prevent the oxidation of powders, milling was performed in an argon environment. A cylindrical die, made of Mo40 steel, with a hole diameter of 15 mm and a VCN 150 resistant steel

punch with a diameter of 15 mm, were used for the consolidation of the ball milled powder. Further, two 5 mm thick cylindrical discs made of the punch's material were used to enhance the surface quality of the compacts and reduce the negative effects of spring-back and ejection force. After the die temperature was stabilized at 450 °C (~0.75 melting point of pure Mg), powders were uniaxially compacted at 600 MPa and held at this pressure for 25 min. The required temperature was provided by a 1200W ceramic heating element and the temperature was constantly measured using a thermometer. After the compaction stage, cylindrical nanocomposite samples with the length of 12 mm and the diameter of 15 mm were prepared for indentation experiments.

To obtain the experimental L–P curves, the instrumented indentation testing was performed on the produced composites according to the ASTM E2546 standard [39]. The experimental set-up and a tested sample are shown in Fig. 1. As the figure depicts, a 5-ton SANTAM hydraulic press was used to push the spherical indenter (Brinell) into the sample to the depth of 0.1 mm. The diameter of the used indenter was 0.1 mm. Fig. 1(b) shows the traces of the indenter on the tested sample. To precisely measure the load variations, an extensometer was used during the indentation experiments.

The load–penetration (L–P) curve obtained in the indentation experiment is directly related to the elastoplastic behavior of the tested material, implying that it can be used to derive the stress–strain ($\sigma$–$\varepsilon$) curve. Fig. 2 demonstrates a typical L–P curve during the indentation test, consisting of loading and unloading stages. A force is applied on a spherical indenter during the loading stage down to a certain indentation depth. The applied force is then removed in the unloading stage, allowing elastic recovery of the tested specimen. While the plastic properties of the tested material are involved in the loading stage, the unloading path is affected by the elastic recovery of the specimen. Therefore, the slope of the loading and unloading paths in an L–P diagram can be used to estimate the plastic flow characteristics and Young's modulus of the material, respectively. For this purpose, a FE model of the indentation test is created and the Hollomon material model with randomly chosen constants is assigned to the tested material. To obtain the true values of the materials constants,

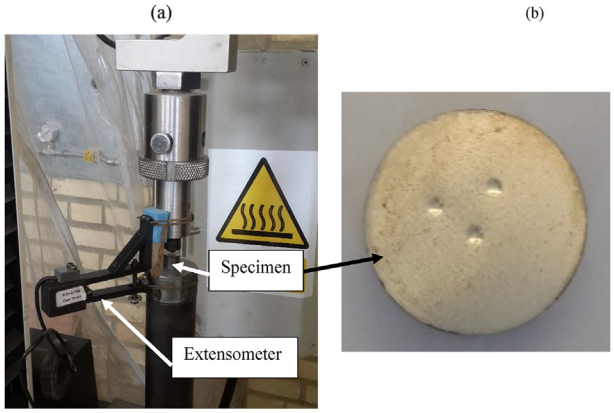


**Fig. 1 – (a) The indentation test set-up, and (b) a tested nanocomposite sample.**

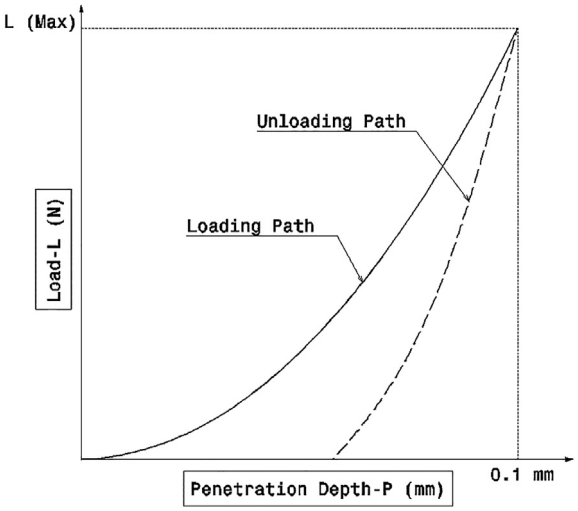


**Fig. 2 – Schematic L–P diagram of the indentation test.**

a neural network is employed to minimize the differences between the experimental and the numerical L–P curves.

## 3. Results and discussions

### 3.1. *Indentation hardness test*

Fig. 3 shows the L–P curves obtained in the indentation test for the produced composites. It is evident from the figure that the applied load increases with the increase in volume content of the reinforcing particles. This can be attributed to the proportional relationship between the strength of the material and the volume content of the reinforcement phase. A similar trend can be observed with the downsizing of the reinforcing particles to nano-scales. A comparison between the results revealed the higher penetration resistance (i.e., hardness) of Mg–$ZrO_2$ compared to similar Mg–$TiO_2$ samples.

### 3.2. *Finite element simulation*

A two-dimensional axial symmetry FE model was developed in Abaqus software to simulate the indentation test (Fig. 4). The indenter was modeled as a rigid body due to its negligible deformation compared to the test specimen [21]. The Hollomon material model was also used to implement the isotropic hardening effect of the composite samples [35]. The Hollomon model is defined as Equation (1):

$$\sigma = \sigma_y^{1-n} E^n \varepsilon^n \tag{1}$$

where $E$, $\sigma_y$, $n$, and $\varepsilon$ are the Young's modulus, yield stress, strain hardening coefficient, and effective strain, respectively.

CAX4R element was used for mesh generation. This element is a 4-node axial symmetry element with reduced formulation and the ability to control the hourglass phenomenon. As the material's properties of the fabricated nanocomposites are unknown, a set of arbitrary values were assigned to the Hollomon material's constants: $E$ = 200 GPa,

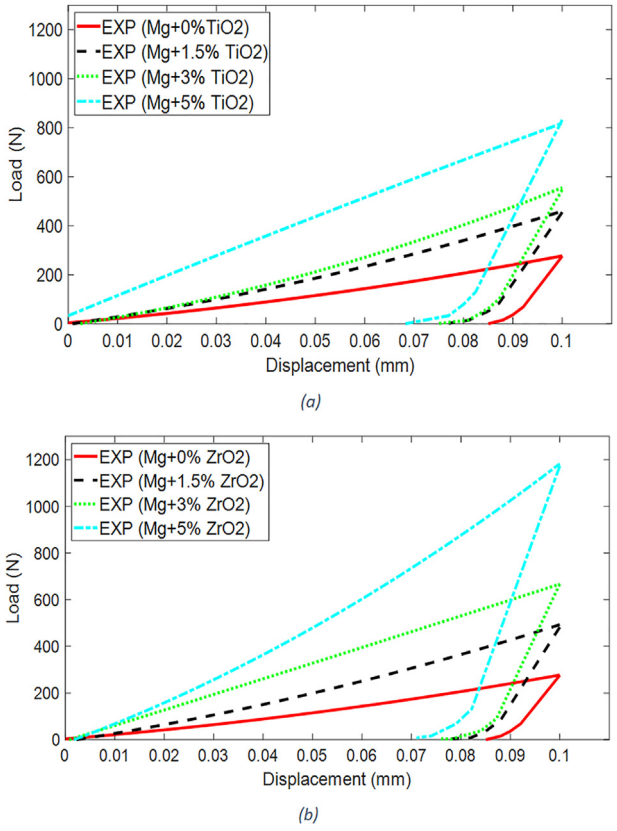


**Fig. 3 – L–P curve of Mg nanocomposites reinforced with $TiO_2$ and $ZrO_2$ nanoparticles.**

$\sigma_y = 200$ MPa, and $n = 0.16$. As the Poisson's ratio has a negligible effect in FE analysis, its value was considered constant and equal to 0.35 for the produced samples [26]. Surface to surface contact with the penalty friction formulation and the friction coefficient of 0.1 [40] were also used to define the contact between the indenter and the test specimen. Based on the mesh convergence analysis (Fig. 5), 22302 CAX4R elements were chosen for meshing.

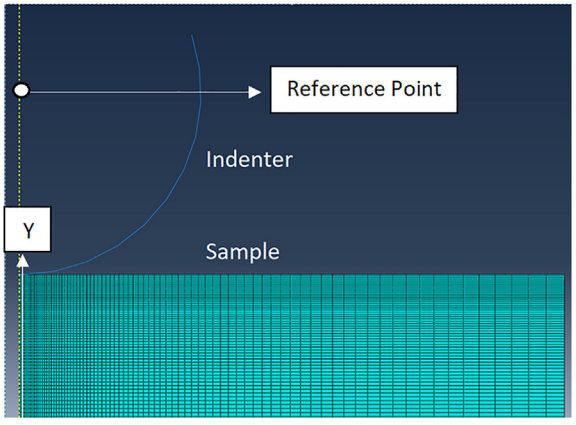


**Fig. 4 – A two-dimensional axial symmetry finite element model in Abaqus software.**

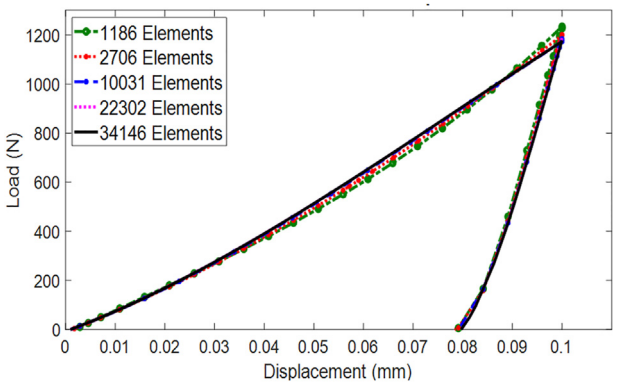


**Fig. 5 – Mesh convergence analysis.**

Appropriate boundary conditions were set according to the real experiment. The bottom surface of the test specimen was fully constrained. The reference point (in Fig. 4) was also constrained in all directions except for the loading direction (Y direction). To apply the loading and un-loading stages, two unidirectional movements were defined for the reference point. At the loading stage, the reference point was moved −0.1 mm in the Y direction and at the un-loading stage, it was moved back +0.1 mm in the same direction to its initial position. The problem was solved for 150 incremental displacements with the pre-defined minimum and maximum increments of 0.005 and 0.5, respectively.

### 3.3. *Artificial neural network (ANN)*

The aim of the developed neural network in this study was to find the Hollomon's equation constants (i.e., $E$, $\sigma_y$, and $n$) for the produced composites. As stated earlier, Young's modulus ($E$) is proportionally related to the slope of the unloading path in the L–P curve [35]. Fig. 6 shows the experimental L–P curves for Mg–5% $TiO_2$ nanocomposite and the L–P curves obtained by the FE simulations at various Young's modulus values and constant yield stress of 200 MPa and strain hardening coefficient of 0.16.

To obtain the Young's modulus of each sample, a parametric study was carried out. The results showed that the E parameter could be approximated using Equation (2):

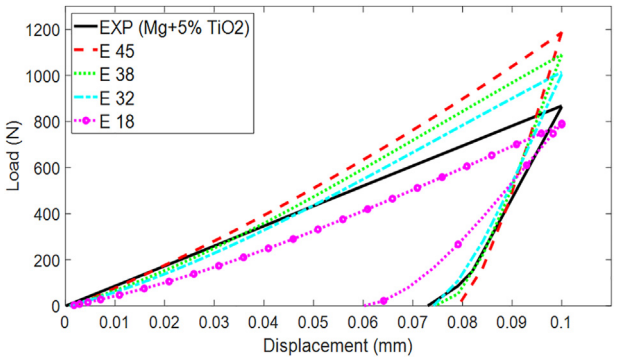


**Fig. 6 – Effect of the Young's modulus on the slope of the loading section.**

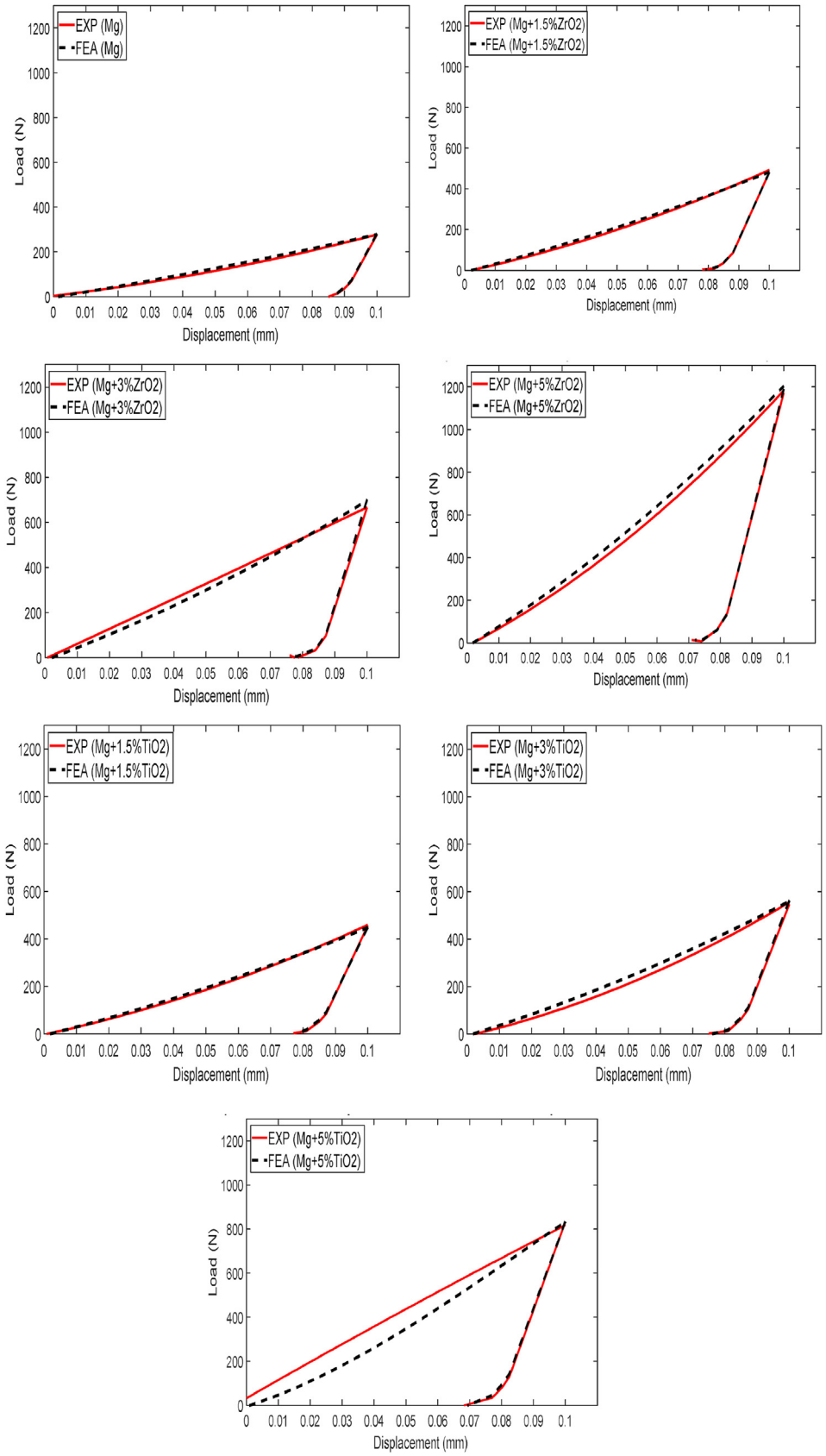


**Fig. 7 – Comparison between the experimental and numerical load–displacement (penetration depth) curves.**

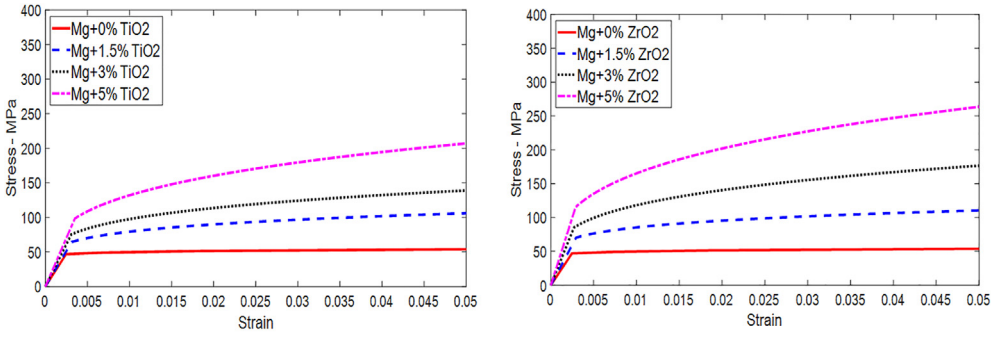


**Fig. 8 – Predicted tensile stress–strain curves for the (a) Mg–$TiO_2$ and (b) Mg–$ZrO_2$ nanocomposites.**

$$y = 1516.9x - 2659.2 \quad (2)$$

In Equation (2), $x$ is the Young's modulus in GPa and y is the slope of the unloading part of the L–P curve in N/mm. The calculated Young's modulus of each sample is presented in Table 1. To train the neural network, the lower and upper bounds of the target parameters ($\sigma_y$ and $n$) were defined as below:

$$\begin{aligned} \sigma_y &= [50, 100, 150, 200, 275, 350] \\ n &= [0.02, 0.08, 0.15, 0.24, 0.34, 0.44] \\ E &= [19.05, 20.53, 23.8, 24.4, 28.02, 31.46, 39.86] \end{aligned} \quad (3)$$

Total work, elastic work, and maximum force were measured from the L–P curves and considered as the input parameters. Considering that the significant difference between the yield stress and the coefficient of strain hardening may cause difficulty in training the neural network, a non-dimensionalization technique using Equation (4) was employed to scale the input and target parameters [41].

$$\begin{aligned} \text{Input} &= \left[\frac{W_t}{Eh_{max}^3}, \frac{F_{max}}{Eh_{max}^2}, \frac{W_e}{Eh_{max}^3}\right] \\ \text{Target} &= \left[\frac{\sigma_y}{E}, n\right] \end{aligned} \quad (4)$$

In total, 252 simulations were performed. 70% of the sample set was used for network training, 15% for network testing, and the remaining 15% for validating the trained network. Levenberg–Marquardt (LM) algorithm was used to train a neural network composed of a hidden layer. Tansig and Purelin transfer functions were also used in the input and the output layers of the network, respectively.

**Table 1 – Material model constants obtained by the developed ANN.**

| Sample | Young's modulus (GPa) | Yield stress (MPa) | Hardness coefficient |
|---|---|---|---|
| Pure Mg | 19.05 | 46.78 | 0.05 |
| Mg + 1.5% $TiO_2$ | 20.53 | 64.40 | 0.18 |
| Mg + 3% $TiO_2$ | 24.40 | 75.30 | 0.22 |
| Mg + 5% $TiO_2$ | 28.02 | 98.50 | 0.28 |
| Mg + 1.5% $ZrO_2$ | 23.80 | 70.20 | 0.16 |
| Mg + 3% $ZrO_2$ | 31.46 | 85.20 | 0.25 |
| Mg + 5% $ZrO_2$ | 39.86 | 115.30 | 0.29 |

### 3.4. *Predicted tensile properties*

Material constants in the Hollomon equation for each composite were calculated using the trained ANN and presented in Table 1.

To validate the accuracy of the developed ANN, materials constants obtained by the trained ANN were used for the FE simulations and the resulting L–P curves were compared to the experimental results. Fig. 7 shows a comparison between the experimental and simulated L–P curves for the fabricated nanocomposites.

As shown in Fig. 7, simulation results are in agreement with the experimental data set, indicating the reliability and accuracy of the employed ANN. At the next step, the constants presented in Table 1 were used to estimate the stress–strain ($\sigma$–$\varepsilon$) curves of the produced samples using Equation (5) [26]:

$$\sigma = \begin{cases} E\varepsilon & \varepsilon > \sigma_y/E \\ \sigma_y^{1-n} E^n \varepsilon^n & \varepsilon > \sigma_y/E \end{cases} \quad (5)$$

The results of $\sigma$–$\varepsilon$ calculations are presented in Fig. 8. The results indicate that the tensile strength of the compacted samples is proportionally related to the volume content of the reinforcement phase, while it is inversely proportional to the size of the reinforcing particles. Similar behavior has been reported for compressive strength of Mg-based nanocomposites [42], showing a similar relationship between the reinforcements and compressive/tensile properties of the produced composites. It is notable that the neural networks are unable to extrapolate the results, implying that they cannot be employed for cases out of the training data set.

## 4. Conclusion

In this study, Mg-based nanocomposites reinforced with $TiO_2$ and $ZrO_2$ nanoparticles were produced by a hot compaction method. As the samples produced by the powder compaction techniques are small for a standard tensile test, an experimental-numerical approach was implemented to evaluate the tensile strength of the produced composites. First,

spherical indentation experiment was performed on the samples and their load–penetration data were recorded as experimental L–P curves. A FE model of the indentation test was then developed using the Hollomon material model for the tested specimens and a simulated L–P curve was obtained for each composite using the simulations. Materials constants of the Hollomon model (yield stress and strain hardening coefficient) were randomly chosen at the first simulation. To obtain the correct material parameters for each of the fabricated composites, the deviation between the experimental and simulated L–P curves has to be minimized. For this purpose, a Levenberg–Marquardt neural network was created. In total, 252 numerical simulations were performed to train the network. To validate the results, L–P curves obtained using the FE simulations were compared to the experimental L–P curves. Finally, tensile stress–strain curves were simulated according to the adjusted materials constants. The results indicated that the proposed approach was accurate and reliable in estimating the tensile properties of Mg-based composites produced by the powder metallurgy technique. It was also observed that the tensile strength of the produced composites increased with the increase in volume content of the reinforcement phase and the decrease in size of the reinforcing particles. Based on the results, Mg-5 vol.% $ZrO_2$ and Mg-5 vol.% $TiO_2$ exhibited 2.5 and 2.1 times higher tensile strengths than that of pure Mg, respectively. The methodology of the present work can be the subject of future research on other composites fabricated by various powder compaction techniques.

## Declaration of Competing Interest

The authors declare that they have no known competing financial interests or personal relationships that could have appeared to influence the work reported in this paper.

## REFERENCES


[1] Liu S, Wang Y, Muthuramalingam T, Anbuchezhiyan G. Effect of B4C and MOS2 reinforcement on micro structure and wear properties of aluminum hybrid composite for automotive applications. Compos B Eng 2019;176:107329.

[2] Fallahdoost H, Nouri A, Azimi A. Dual functions of TiC nanoparticles on tribological performance of Al/graphite composites. J Phys Chem Solid 2016;93:137–44.

[3] Ramkumar K, Sivasankaran S, Al-Mufadi FA, Siddharth S, Raghu R. Investigations on microstructure, mechanical, and tribological behaviour of AA 7075-x wt.% TiC composites for aerospace applications. Arch Civ Mech Eng 2019;19:428–38.

[4] Dutta S, Gupta S, Roy M. Recent developments in magnesium metal–matrix composites for biomedical applications: a review. ACS Biomater Sci Eng 2020;6:4748–73.

[5] Nouri A, Wen C. Introduction to surface coating and modification for metallic biomaterials, surface coating and modification of metallic biomaterials. 2015. p. 3–60.

[6] Geffroy PM, Chartier T, Silvain JF. Innovative approach to metal matrix composites film by tape casting process. Adv Eng Mater 2007;9:547–53.

[7] Rahmani K, Majzoobi G, Ebrahim-Zadeh G, Kashfi M. Comprehensive study on quasi-static and dynamic mechanical properties and wear behavior of Mg—B4C composite compacted at several loading rates through powder metallurgy. Trans Nonferrous Metals Soc China 2021;31:371–81.

[8] Nouri A, Sola A. Metal particle shape: a practical perspective. Met Powder Rep 2018;73:276–82.

[9] Rahmani K, Sadooghi A, Hashemi S. The effect of Al2O3 content on tribology and corrosion properties of Mg-Al2O3 nanocomposites produced by single and double-action press. Mater Chem Phys 2020;250:123058.

[10] Rahmani K, Majzoobi G. The effect of particle size on microstructure, relative density and indentation load of Mg-B4C composites fabricated at different loading rates. J Compos Mater 2020;54:2297–311.

[11] Rahmani K, Majzoobi GH, Bakhtiari H, Sadooghi A. On the effect of compaction velocity, size, and content of reinforcing particles on corrosion resistance of Mg–B4C composites. Mater Chem Phys 2021;271:124946.

[12] Majzoobi G, Rahmani K, Kashfi M. The effect of pre-compaction on properties of Mg/SiC nanocomposites compacted at high strain rates. J Stress Anal 2020;4:19–28.

[13] Rahmani K, Sadooghi A, Hashemi SJ. The effect of cold and hot pressing on mechanical properties and tribological behavior of Mg-Al2O3 nanocomposites. Mater Res Express 2020;7:085012.

[14] Nazari KA, Hilditch T, Dargusch MS, Nouri A. Functionally graded porous scaffolds made of Ti-based agglomerates. J Mech Behav Biomed Mater 2016;63:157–63.

[15] Rahmani K, Sadooghi A, Nokhberoosta M. The effect of the double-action pressure on the physical, mechanical and tribology properties of Mg-WO3 nanocomposites. J Mater Res Technol 2020;9:1104–18.

[16] Abdollahi A, Alizadeh A, Baharvandi HR. Dry sliding tribological behavior and mechanical properties of Al2024–5 wt.% B4C nanocomposite produced by mechanical milling and hot extrusion. Mater Des 2014;55:471–81.

[17] Sudha G, Stalin B, Ravichandran M, Balasubramanian M. Mechanical properties, characterization and wear behavior of powder metallurgy composites-a review. Mater Today: Proc 2020;22:2582–96.

[18] El-Daly A, Abdelhameed M, Hashish M, Eid A. Synthesis of Al/SiC nanocomposite and evaluation of its mechanical properties using pulse echo overlap method. J Alloys Compd 2012;542:51–8.

[19] El-Daly A, Abdelhameed M, Hashish M, Daoush WM. Fabrication of silicon carbide reinforced aluminum matrix nanocomposites and characterization of its mechanical properties using non-destructive technique. Mater Sci Eng A 2013;559:384–93.

[20] Collin J-M, Mauvoisin G, Bartier O, El Abdi R, Pilvin P. Experimental evaluation of the stress–strain curve by continuous indentation using different indenter shapes. Mater Sci Eng A 2009;501:140–5.

[21] Mahmoudi A, Nourbakhsh S, Amali R. An alternative approach to determine material characteristics using spherical indentation and neural networks for bulk metals. J Test Eval 2012;40:211–9.

[22] Jones RM. Mechanics of composite materials. CRC Press; 1998.

[23] Nayebi A, El Abdi R, Bartier O, Mauvoisin G. New procedure to determine steel mechanical parameters from the spherical indentation technique. Mech Mater 2002;34:243–54.

[24] Oliver WC, Pharr GM. An improved technique for determining hardness and elastic modulus using load and displacement sensing indentation experiments. J Mater Res 1992;7:1564–83.

[25] Lai M, Lim K. On the prediction of tensile properties from hardness tests. J Mater Sci 1991;26:2031–6.

[26] Beghini M, Bertini L, Fontanari V. Evaluation of the stress–strain curve of metallic materials by spherical indentation. Int J Solid Struct 2006;43:2441–59.
[27] Collin J-M, Mauvoisin G, El Abdi R. An experimental method to determine the contact radius changes during a spherical instrumented indentation. Mech Mater 2008;40:401–6.
[28] Noii N, Aghayan I. Characterization of elastic-plastic coated material properties by indentation techniques using optimisation algorithms and finite element analysis. Int J Mech Sci 2019;152:465–80.
[29] Chen G, Zhong J, Zhang X, Guan K, Wang Q, Shi J. Estimation of tensile strengths of metals using spherical indentation test and database. Int J Pres Ves Pip 2021;189:104284.
[30] Khatir S, Boutchicha D, Le Thanh C, Tran-Ngoc H, Nguyen T, Abdel-Wahab M. Improved ANN technique combined with Jaya algorithm for crack identification in plates using XIGA and experimental analysis. Theor Appl Fract Mech 2020;107:102554.
[31] Zenzen R, Khatir S, Belaidi I, Le Thanh C, Wahab MA. A modified transmissibility indicator and Artificial Neural Network for damage identification and quantification in laminated composite structures. Compos Struct 2020;248:112497.
[32] Tran-Ngoc H, Khatir S, Le-Xuan T, De Roeck G, Bui-Tien T, Wahab MA. A novel machine-learning based on the global search techniques using vectorized data for damage detection in structures. Int J Eng Sci 2020;157:103376.
[33] Wang S, Wang H, Zhou Y, Liu J, Dai P, Du X, et al. Automatic laser profile recognition and fast tracking for structured light measurement using deep learning and template matching. Measurement 2021;169:108362.
[34] Jeong K, Lee H, Kwon OM, Jung J, Kwon D, Han HN. Prediction of uniaxial tensile flow using finite element-based indentation and optimized artificial neural networks. Mater Des 2020;196:109104.
[35] Atrian A, Majzoobi G, Nourbakhsh S, Galehdari S, Nejad RM. Evaluation of tensile strength of Al7075-SiC nanocomposite compacted by gas gun using spherical indentation test and neural networks. Adv Powder Technol 2016;27:1821–7.
[36] Huber N, Konstantinidis A, Tsakmakis C. Determination of Poisson's ratio by spherical indentation using neural networks—Part I: Theory. J Appl Mech 2001;68:218–23.
[37] Kucharski S, Mróz Z. Identification of yield stress and plastic hardening parameters from a spherical indentation test. Int J Mech Sci 2007;49:1238–50.
[38] Rahmani K, Majzoobi G, Sadooghi A, Kashfi M. Mechanical and physical characterization of Mg-TiO2 and Mg-ZrO2 nanocomposites produced by hot-pressing. Mater Chem Phys 2020;246:122844.
[39] E. ASTM, 2546–07, Standard practice for instrumented indentation testing.
[40] Borodich FM, Keer LM. Contact problems and depth-sensing nanoindentation for frictionless and frictional boundary conditions. Int J Solid Struct 2004;41:2479–99.
[41] Hosseinzadeh A, Mahmoudi A. Determination of mechanical properties using sharp macro-indentation method and genetic algorithm. Mech Mater 2017;114:57–68.
[42] Majzoobi GH, Rahmani K. Mechanical characterization of Mg-B 4 C nanocomposite fabricated at different strain rates. Int J Miner Metall Mater 2020;27:252–63.